

ProtoOcc: Accurate, Efficient 3D Occupancy Prediction Using Dual Branch Encoder-Prototype Query Decoder

Jungho Kim^{1*} Changwon Kang^{2*} Dongyoung Lee^{2*} Sehwan Choi² Jun Won Choi^{1†}

¹Seoul National University ²Hanyang University

Abstract

In this paper, we introduce ProtoOcc, a novel 3D occupancy prediction model designed to predict the occupancy states and semantic classes of 3D voxels through a deep semantic understanding of scenes. ProtoOcc consists of two main components: the *Dual Branch Encoder* (DBE) and the *Prototype Query Decoder* (PQD). The DBE produces a new 3D voxel representation by combining 3D voxel and BEV representations across multiple scales through a dual branch structure. This design enhances both performance and computational efficiency by providing a large receptive field for the BEV representation while maintaining a smaller receptive field for the voxel representation. The PQD introduces Prototype Queries to accelerate the decoding process. Scene-Adaptive Prototypes are derived from the 3D voxel features of input sample, while Scene-Agnostic Prototypes are computed by applying Scene-Adaptive Prototypes to an Exponential Moving Average during the training phase. By using these prototype-based queries for decoding, we can directly predict 3D occupancy in a single step, eliminating the need for iterative Transformer decoding. Additionally, we propose the *Robust Prototype Learning*, which injects noise into prototype generation process and trains the model to denoise during the training phase. ProtoOcc achieves state-of-the-art performance with 45.02% *mIoU* on the Occ3D-nuScenes benchmark. For single-frame method, it reaches 39.56% *mIoU* with an inference speed of 12.83 FPS on an NVIDIA RTX 3090. Our code can be found at <https://github.com/SPA-junghokim/ProtoOcc>

1. Introduction

Vision-based 3D occupancy prediction is a critical task for comprehensive scene understanding around the ego vehicle in autonomous driving. This task aims to simultaneously estimate occupancy states and semantic classes using multi-view images in 3D space, providing detailed 3D scene information. The typical prediction pipeline of previous methods comprises three main components: 1) a view transformation module, 2) an encoder, and 3) a decoder. Initially, feature maps extracted from multi-view images are transformed into 3D spatial representations through a 2D-to-3D view transformation. An encoder network then processes these 3D rep-

*Equal contributions

†Corresponding author

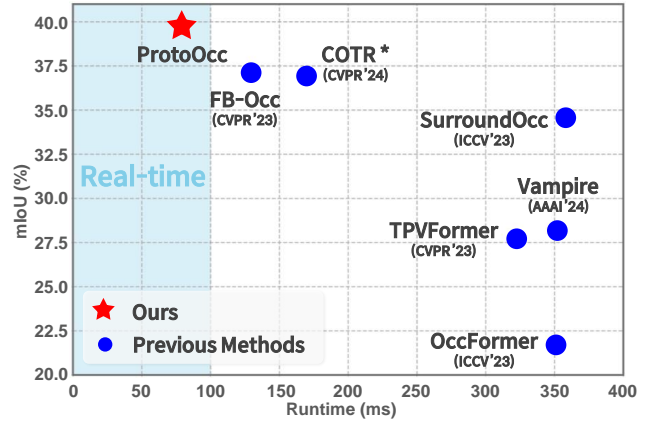


Figure 1: Comparisons of the *mIoU* and runtime on the Occ3D-nuScenes validation set. The "★" indicates results reproduced using public codes. Inference time is measured on a single NVIDIA RTX 3090 GPU.

resentations to produce high-level semantic spatial features, capturing the overall scene context. Finally, a decoder network utilizes these encoded 3D spatial features to predict semantic occupancy for all voxels composing the scene.

Existing works have explored enhancing encoder-decoder networks to improve both the accuracy and computational efficiency of 3D occupancy prediction. Various attempts have been made to optimize encoders using 3D spatial representations. Figure 2 (a) illustrates two commonly used 3D representations, including voxel representation [15, 26, 28] and Bird's-Eye View (BEV) representation [12, 32]. Voxel-based encoding methods [36, 4] utilize 3D Convolution Neural Networks (CNNs) to encode voxel structures. However, due to the large number of voxels required to cover 3D surroundings, this approach demands significant memory and computational resources. One way to reduce this complexity is by decreasing the capacity of 3D CNNs, but this comes at the cost of a reduced receptive field, which can limit overall performance.

In contrast, BEV representation projects 3D information onto a 2D plane, significantly reducing memory and computational demands compared to voxel representation. After encoding the BEV representation using 2D CNNs, it is con-

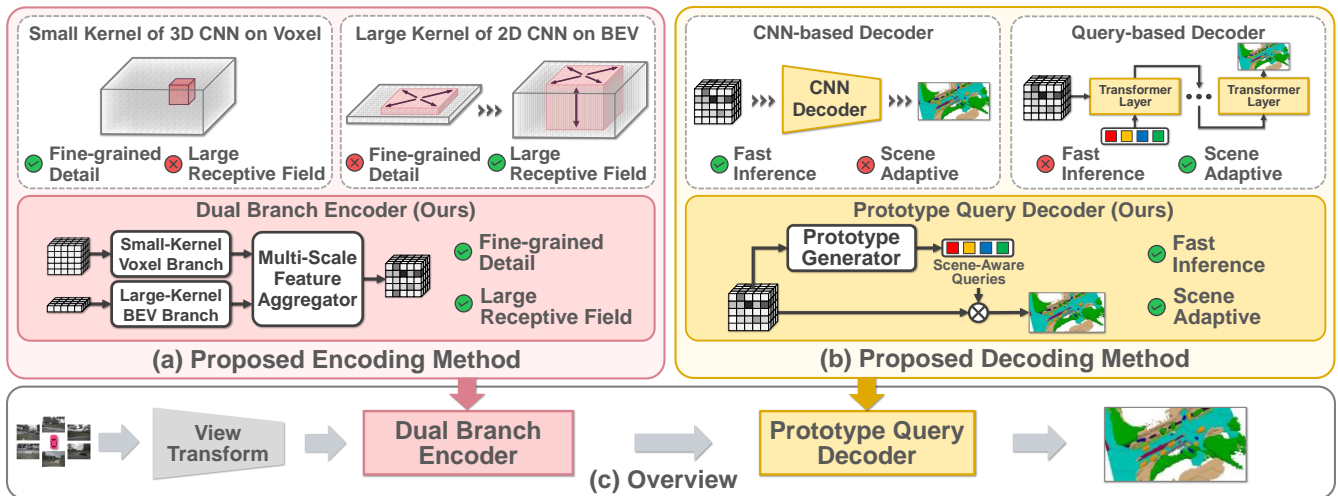


Figure 2: Overall structure of ProtoOcc. (a) Dual Branch Encoder captures fine-grained 3D structures and models the large receptive fields in voxel and BEV domains, respectively. (b) The Prototype Query Decoder generates Scene-Aware Queries utilizing prototypes and achieves fast inference without iterative query decoding. (c) Our ProtoOcc framework integrates Dual Branch Encoder and Prototype Mask Decoder for 3D occupancy prediction.

verted back to a 3D voxel structure for 3D occupancy prediction. However, this approach lacks detailed 3D geometric information due to the reduction in height dimensionality. While BEV representation can be improved by incorporating additional 3D information [12, 32], its performance impact is still constrained by the inherent limitations of representing 3D scenes in a 2D format.

Another line of research focuses on enhancing the decoders. As illustrated in Figure 2 (b), two main decoding strategies exist: 1) CNN-based decoders [4, 38, 31, 34] and 2) query-based decoders [36, 23, 19]. CNN-based decoders employ lightweight 3D CNNs to extract semantic voxel features, while query-based decoders iteratively decode a query using the 3D representation obtained from the encoder. Although query-based decoders can achieve better prediction accuracy, they require processing through multiple decoding layers, leading to higher computational complexity and increased inference time. Therefore, it is crucial to reduce this complexity while retaining the performance benefits of query-based decoders.

To address the aforementioned challenges, we introduce ProtoOcc, an efficient encoder-decoder framework for a 3D occupancy prediction network. As shown in Figure 1, ProtoOcc achieves state-of-the-art (SOTA) performance while achieving relatively fast inference (i.e., 77.9 ms) on a single NVIDIA RTX 3090 GPU.

As shown in Figure 2 (a), ProtoOcc utilizes a *Dual Branch Encoder* (DBE) with a dual-branch architecture. While the voxel branch generates voxel features using 3D CNNs with a small kernel size, the BEV branch produces BEV features using 2D CNNs with a large kernel size. The BEV and voxel features are fused across multiple scales, resulting in Comprehensive Voxel Features. This design reduces the complexity typically associated with 3D CNNs while effectively increasing the receptive field at a lower

computational cost. Furthermore, this dual encoding approach efficiently captures both fine-grained 3D structures and long-range spatial relationships across various scales.

Recognizing that query-based decoding requires high computational complexity due to processing over multiple decoding layers, we introduce the *Prototype Query Decoder* (PQD) to accelerate the decoding process. PQD eliminates the need for iterative decoding by employing prototype-based queries that can directly produce prediction results in a single step. To this end, we generate Scene-Adaptive Prototypes derived from the Comprehensive Voxel Features of the input sample. While prototypes can be computed for the semantic classes present in the input, challenges arise when certain semantic classes are missing. To address this, we also devise Scene-Agnostic Prototypes, which are obtained by filtering Scene-Adaptive Prototypes with an Exponential Moving Average (EMA) method during the training phase. PQD then merges Scene-Adaptive Prototypes with Scene-Agnostic Prototypes to form Scene-Aware Queries. Note that Scene-Aware Queries are used to perform 3D occupancy prediction directly.

We also develop a novel training method for enhancing the performance of the proposed decoder. Since the prototypes are directly utilized for 3D occupancy prediction without an iterative query decoding, the quality of the prototypes significantly impacts the overall performance. To ensure robust predictions, we devise the *Robust Prototype Learning* framework that injects noise into the prototype generation process and trains the model to counteract this noise during the training phase.

We evaluated ProtoOcc on the challenging Occ-3D nuScenes benchmark [24]. ProtoOcc achieves an *mIoU* of **39.56%**, surpassing the performance of all existing single-frame methods, while operating at a processing speed of **12.83 FPS** on an NVIDIA RTX 3090. ProtoOcc with multi-

frame temporal fusion also achieves SOTA performance among previous multi-frame methods, with an *mIoU* of **45.02%**.

The contributions of this study are summarized below:

- We introduce ProtoOcc, a novel 3D occupancy prediction model that enhances both the performance and efficiency of the encoding and decoding processes.
- We propose an enhanced 3D representation for the encoder that combines voxel and BEV scene representations through dual branch pipelines. This DBE method efficiently allocates resources, forming the largest receptive field with minimal computational cost.
- We propose a computationally efficient decoder performing 3D occupancy prediction in a single pass. This PQD generates queries representing each class from the encoded 3D spatial features and directly predicts semantic occupancy without a decoding process, thereby significantly reducing the computational complexity.
- ProtoOcc achieves state-of-the-art performance, with a 45.02% *mIoU* on the Occ-3D benchmark. It also achieves a 39.56% *mIoU* at a processing speed of 12.83 FPS.
- The codes will be publicly available.

2. Related Works

2.1. Encoder for 3D Occupancy Prediction

3D occupancy prediction [25] has attracted considerable interest in recent years due to its ability to reconstruct 3D volumetric scene structures from multi-view images. These methods typically encode 3D representations such as voxels or a BEV transformed from images [22, 16]. MonoScene [4] is the first method to predict 3D semantic occupancy using only an image, encoding the 3D voxel representations by utilizing a 3D UNet in outdoor environments. OccFormer [36] divides 3D representations into voxel and BEV forms to effectively process the 3D volume and then encodes them through shifted window-based attention. FastOcc [12] integrates BEV features extracted by a lightweight 2D CNN with 3D voxel features interpolated from image features.

2.2. Decoder for 3D Occupancy Prediction

Recent methods [37, 3, 19, 23] have introduced query-based decoders that use queries to capture scene-adaptive features by interacting queries and voxel features. OccFormer [36] adapts Mask2Former’s [7] 2D mask decoder to 3D space for occupancy prediction, iteratively decoding queries through masked attention between queries and voxels. COTR [21] uses a coarse-to-fine semantic grouping strategy to address class imbalance by dividing categories into groups with different ground truth supervision.

2.3. Large Receptive Fields in 2D Domain

The large receptive field has been a crucial factor in perception tasks due to its ability to capture global context. Recent studies [9, 30] have demonstrated that a large receptive field

Kernel Size		$k = 3$	$k = 5$	$k = 7$	$k = 9$	$k = 11$
3D	FLOPs	69.1M	320.0M	878.1M	1.9G	3.4G
	Latency (ms)	13.1	15.8	20.6	27.3	39.5
2D	FLOPs	2.9M	8.0M	15.6M	25.9M	38.7M
	Latency (ms)	0.833	0.868	0.899	0.934	0.988

Table 1: Comparison of 2D and 3D convolution with varying kernel sizes. The k denotes the kernel size for each convolution layer. Both layers have 32 input and output channels. The 3D layer uses a $200 \times 200 \times 16$ voxel size, while the 2D layer uses a 200×200 BEV size.

contributes to which have been widely adopted Transformer-based models in perception tasks [33, 10].

Similarly, CNN-based models with large receptive fields have been shown to achieve performance comparable to Transformer-based architectures. ConvNeXt [20] adopts 7×7 depth-wise convolution and increases capacity using an inverted bottleneck architecture with Multi-Layer Perceptron (MLP) blocks. RepLKNet [8] employs a re-parameterization method to efficiently utilize large-size kernels up to 31×31 . LargeKernel3D [6] efficiently implements 3D convolution with large kernel size by sharing weights among spatially adjacent locations within the kernel.

3. ProtoOcc

3.1. Overview

The overall architecture of ProtoOcc is illustrated in Figure 2 (c). Initially, a 2D-to-3D view transformation generates both 3D voxel and BEV features from multi-view camera images. DBE then combines these features across multiple scales to produce Comprehensive Voxel Features. Next, PQD computes scene-aware prototypes from the current scene. It initializes the queries using both Scene-Adaptive and Scene-Agnostic Prototypes and performs dot product operation between the queries and Comprehensive Voxel Features to predict 3D occupancy.

2D-to-3D View Transformation. The 2D-to-3D View transformation process employs the Lift-Splat-Shoot (LSS) method [22] to convert multi-view camera inputs into 3D features in both voxel and BEV formats. 2D feature maps are extracted from multi-view images using a backbone network such as ResNet [11]. These features are then fed into a depth network to predict depth distributions. Frustum features are generated by computing the outer product between 2D feature maps and depth distributions. The voxel-pooling method transforms these frustum features into a unified 3D voxel feature F_{vox} . Finally, the BEV feature F_{BEV} is reshaped from F_{vox} along the channel dimension, changing from (D, X, Y, Z) to $(D \times Z, X, Y)$, where D denotes the channel dimension and (X, Y, Z) represents the volume scale.

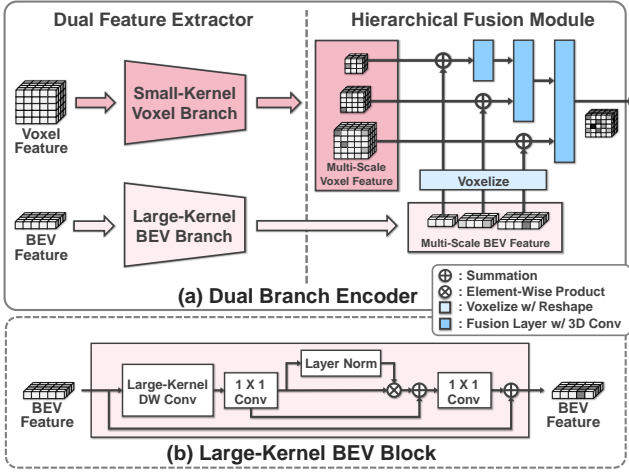


Figure 3: Details of Dual Branch Encoder. (a) DBE consists of DFE and HFM. DFE extracts multi-scale features using the dual encoders in the voxel and BEV domain. HFM hierarchically aggregates these features from low to high scales into Comprehensive Voxel Features. (b) The Large-Kernel BEV Block comprises a large kernel depth-wise convolution, 1x1 convolutions, and layer normalization.

3.2. Dual Branch Encoder

The overall architecture of DBE is depicted in Figure 3 (a). DBE consists of two main components: the *Dual Feature Extractor* (DFE) and the *Hierarchical Fusion Module* (HFM). DFE extracts multi-scale dual features to capture fine-grained 3D structures and long-range spatial relationships in the voxel and BEV domains, respectively. HFM hierarchically aggregates multi-scale dual features to generate comprehensive context features at various levels of detail.

Dual Feature Extractor. DFE consists of a voxel branch using 3D CNNs with a small kernel size and a BEV branch using 2D CNNs with a large kernel size, where each branch is designed to extract multi-scale features. In this dual branch framework, the 2D representation F_{BEV} is derived by reshaping F_{vox} along the channel dimension to incorporate height information, thereby integrating 3D information. DFE expands the 3D receptive field by increasing the kernel size of 2D CNNs in the BEV domain, reducing the complexity associated with 3D CNNs while achieving expansion at a lower computational cost. Table 1 demonstrates the significant computational efficiency of this approach by showing that expanding kernel sizes in 3D convolution substantially increases computational costs, whereas it results in only minimal latency increases in 2D convolution.

To extract the multi-scale features for each domain, F_{vox} is processed through downsampling layers based on small-kernel 3D CNNs for fine-grained 3D structures. This process yields $\mathbf{V}^{vox} = \{V_i^{vox} \in \mathbb{R}^{D_i \times X_i \times Y_i \times Z_i}\}_{i=1}^S$, where i denotes the scale index and S represents the total number of scales. In parallel, multi-scale BEV features $\mathbf{B}^{BEV} = \{B_i^{BEV} \in \mathbb{R}^{D'_i \times X_i \times Y_i}\}_{i=1}^S$ are extracted by F_{BEV} in a similar manner to the voxel feature extraction process. The key

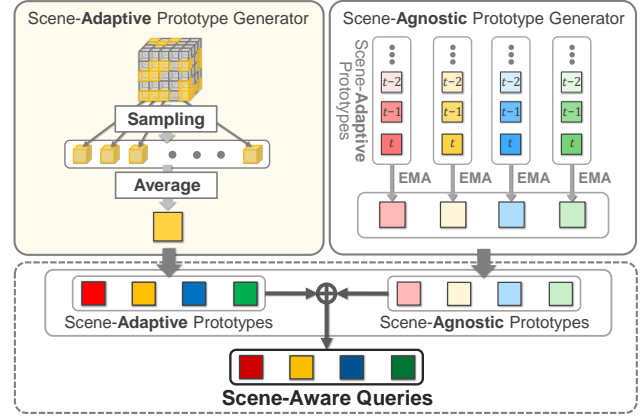


Figure 4: Details of prototype generation. AdaPG generates Scene-Adaptive Prototypes by sampling and averaging Comprehensive Voxel Features for each class based on class-specific masks. AgnoPG generates Scene-Agnostic Prototypes by leveraging Scene-Adaptive Prototypes through the EMA method. Finally, Scene-Adaptive Prototypes and Scene-Agnostic Prototypes are combined into Scene-Aware Queries.

difference is the use of 2D CNNs with large kernels (see Figure 3 (b)) to consider long-range dependencies inspired by ConvNeXt [20, 29].

Hierarchical Fusion Module. HFM integrates voxel and BEV information across multiple scales, leveraging the strengths of both representations to generate Comprehensive Voxel Features. The multi-scale dual features are aggregated through sequential processing with a series of up-sampling layers, followed by a 3D CNN. In each layer, the BEV feature B_i^{BEV} at the i -th scale is voxelized into $V_i^{BEV} \in \mathbb{R}^{D_i \times X_i \times Y_i^j \times Z_i}$ through reshaping operation. Subsequently, the fused voxel feature V_i^{fused} is derived by aggregating the voxel feature V_i^{vox} , the voxelized BEV feature V_i^{BEV} , and the upsampled fused voxel feature $Up(V_{i-1}^{fused})$ from the previous layer as follows:

$$V_i^{fused} = \begin{cases} Conv(Up(V_{i-1}^{fused}) + V_i^{BEV} + V_i^{vox}) & \text{if } i > 1 \\ Conv(V_i^{BEV} + V_i^{vox}) & \text{otherwise} \end{cases}, \quad (1)$$

where Up denotes upsampling layer by trilinear interpolation and $Conv$ denotes a 3D convolution layer with a small kernel size. After processing through S upsampling layers, DBE ends up with Comprehensive Voxel Features $V_{CVF} = V_S^{fused}$.

3.3. Prototype Query Decoder

As illustrated in Figure 4, PQD comprises two components: the *Scene-Adaptive Prototype Generator* (AdaPG) and the *Scene-Agnostic Prototype Generator* (AgnoPG). The AdaPG generates Scene-Adaptive Prototypes to capture the unique features of each class in the current scene. The AgnoPG produces Scene-Agnostic Prototypes representing generalized features for all individual classes across differ-

ent scenes through the EMA method [2]. Finally, PQD predicts semantic occupancy for all voxels by performing dot product operations between the Comprehensive Voxel Features and the queries generated from the prototypes by the AdaPG and the AgnoPG.

Scene-Adaptive Prototype Generator. AdaPG generates Scene-Adaptive Prototypes to capture the unique semantics of each class present in the current scene. Specifically, the AdaPG uses a shallow 3D CNN classifier to produce voxel-wise class probabilities $O_s \in \mathbb{R}^{C \times X \times Y \times Z}$, where C denotes the number of semantic categories, including the empty class. The O_s is then used to generate class-specific masks $M^{cls} = \{M_c^{cls} \in \{0, 1\}^{X \times Y \times Z}\}_{c=1}^C$ by assigning each voxel to the class with the highest probability. These class-specific masks are generated to sample the voxel features for each class as formulated below:

$$M_c^{cls}(x, y, z) = \begin{cases} 1 & \text{if } \underset{c}{\operatorname{argmax}} O_s(x, y, z) = c \\ 0 & \text{otherwise} \end{cases}. \quad (2)$$

The Scene-Adaptive Prototypes $\mathbf{P}^d = \{P_c^d \in \mathbb{R}^D\}_{c=1}^C$ are then computed by average pooling in the x , y , and z domains:

$$P_c^d = \frac{1}{N_c^{nz}} \sum_{x, y, z} (M_c^{cls}(x, y, z) \otimes V_{CVF}(x, y, z)), \quad (3)$$

where N_c^{nz} denotes the number of non-zero voxels in M_c^{cls} and \otimes is the element-wise product. In case where N_c^{nz} is zero, the prototype P_c^d is initialized to zero vector. The resulting \mathbf{P}^d are subsequently used in the AgnoPG and query generation.

Scene-Agnostic Prototype Generator. While AdaPG effectively captures class-specific features within an input sample, it has the limitation of potentially missing certain classes. To address this, the AgnoPG generates Scene-Agnostic Prototypes $\mathbf{P}^g = \{P_c^g \in \mathbb{R}^D\}_{c=1}^C$ by leveraging \mathbf{P}^d through the EMA method. This process is designed to capture consistent and generalized features for all individual classes, even those absent from the current sample. \mathbf{P}^g is gradually updated by integrating \mathbf{P}^d from multiple samples, with a focus on the classes present in each sample. Consequently, the \mathbf{P}^g is formulated as follows:

$$\mathbf{P}^g(t) = \alpha \cdot \mathbf{P}^d(t) + (1 - \alpha) \cdot \mathbf{P}^g(t - 1), \quad (4)$$

where t denotes the current training iteration and α is the EMA coefficient.

Prototype-Driven Occupancy Prediction. PQD generates Scene-Aware Queries $Q^{SA} \in \mathbb{R}^{C \times D}$ by summing \mathbf{P}^d and \mathbf{P}^g , followed by processing through an MLP. These queries provide comprehensive features that capture unique and consistent class properties. The resulting Q^{SA} is then used to predict semantic logits. Subsequently, the occupancy masks are obtained by applying a dot product operation between Comprehensive Voxel Features and Q^{SA} along the channel dimension, and a sigmoid function is applied to normalize the masks. Similar to [36], the final 3D semantic

occupancy prediction is computed by leveraging the occupancy masks and the semantic logits. This approach eliminates the need for iterative decoding by generating queries derived from Comprehensive Voxel Features. The queries generated by the prototypes directly and efficiently predict semantic occupancy in a single step.

3.4. Training

Robust Prototype Learning. ProtoOcc generates Scene-Adaptive Prototypes \mathbf{P}^d using class-specific masks M^{cls} from AdaPG. When using inaccurate masks to average pool voxel features for each class, features from voxels actually belonging to different classes are included. This prevents prototypes from accurately representing each class’s unique features, degrading prediction accuracy.

To address this issue, we introduce Robust Prototype Learning (RPL), inspired by [35, 5]. RPL adds noise to M^{cls} to generate Noisy Scene-Adaptive Prototypes $\hat{\mathbf{P}}^d$, which are combined with \mathbf{P}^g to produce Noisy Scene-Aware Queries \hat{Q}^{SA} . These queries are concatenated with Q^{SA} and then independently predict voxel occupancy and class. This process trains the model to denoise \hat{Q}^{SA} , enabling robust occupancy predictions even when M^{cls} are inaccurate. This approach, applied during the training phase, enhances the model’s capabilities without affecting inference time.

For enhanced robustness in 3D scene understanding, we introduce two types of noise, scaling noise and random flipping noise. Scaling noise adjusts the size of M^{cls} based on the ego vehicle’s position, addressing depth ambiguity. Random flipping noise reallocates voxel grid classes randomly, mitigating the misclassification of similar classes, such as trailers and trucks.

Training Loss. The total loss \mathcal{L}_{total} used to train ProtoOcc is given by

$$\mathcal{L}_{total} = \mathcal{L}_{depth} + \mathcal{L}_{AdaPG} + \mathcal{L}_{occ} + \mathcal{L}_{RPL}, \quad (5)$$

where \mathcal{L}_{depth} is for depth estimation, \mathcal{L}_{AdaPG} is for class-specific mask prediction in AdaPG, \mathcal{L}_{occ} is for query-based occupancy prediction, and \mathcal{L}_{RPL} is for the Robust Prototype Learning. Specifically, \mathcal{L}_{depth} uses LiDAR point clouds projected onto the image, employing cross-entropy (CE) loss. \mathcal{L}_{AdaPG} includes Lovasz [1] and Dice losses for class-specific mask prediction used in Scene-Adaptive Prototypes generation. \mathcal{L}_{occ} is calculated without a bipartite matching process, with queries equal to the number of classes. This loss uses CE loss for classification and focal loss [18] combined with dice loss for mask prediction. \mathcal{L}_{RPL} uses the same functions as \mathcal{L}_{occ} for the \hat{Q}^{SA} in RPL.

4. Experiments

4.1. Experimental Settings

Dataset and Metrics. We conduct the experiments on the Occ3D dataset [24], which evaluates the mean Intersection over Union (*mIoU*) for 17 semantic categories. Furthermore, we measure the latency to assess the model’s efficiency.

Method	Venue	Image Backbone	Image Size	mIoU (%)	Latency (ms)
MonoScene[4]	CVPR'22	ResNet-101	928 × 1600	6.06	830.1
TPVFormer[14]	CVPR'23	ResNet-101	928 × 1600	27.83	320.8
Vampire[31]	AAAI'24	ResNet-101	256 × 704	28.30	349.2
CTF-Occ[24]	NIPS'23	ResNet-101	928 × 1600	28.53	-
SurroundOcc[28]	ICCV'23	ResNet-101	800 × 1333	34.40	355.6
BEVDet[13]	arXiv'21	ResNet-50	256 × 704	19.38	-
OccFormer[36]	ICCV'23	ResNet-50	928 × 1600	21.93	349.2
FastOcc[12]	ICRA'24	ResNet-50	320 × 800	34.21	62.8 †
COTR [21]	CVPR'24	ResNet-50	256 × 704	37.02*	168.9
FB-Occ[17]	ICCV'23	ResNet-50	256 × 704	37.39	129.7
Ours	-	ResNet-50	256 × 704	39.56	77.9

Table 2: Comparison with single-frame methods on the Occ3D-nuScenes validation set. Latency is measured on a single NVIDIA RTX 3090 GPU. The "-" denotes that the associated results are not available. The "†" denotes that the latency was measured on an NVIDIA V100 GPU as reported in the paper. The "*" indicates results reproduced using public code.

Method	Venue	Image Backbone	Image Size	mIoU
BEVFormer	ECCV'22	ResNet-101	928×1600	26.88
PanoOcc	CVPR'24	ResNet-101	864×1600	42.13
BEVDet4D	arXiv'21	ResNet-50	384×704	39.25
FB-Occ	ICCV'23	ResNet-50	256×704	40.69
COTR	CVPR'24	ResNet-50	256×704	44.45
Ours	-	ResNet-50	256×704	45.02

Table 3: Comparison with multi-frame methods on the Occ3D-nuScenes validation set.

Implementation Details. We utilized ResNet-50 [11] for the image backbone network. Our model was trained for 24 epochs with a total batch size of 16 on 4 NVIDIA RTX 3090 GPUs. The AdamW optimizer was employed with a learning rate of 4×10^{-4} for single-frame and 2×10^{-4} for multi-frame.

4.2. Performance Comparison

Table 2 presents a detailed comparison of single-frame methods on the Occ3D-nuScenes validation set, demonstrating our method’s superior performance. Our approach achieves noteworthy results of 39.56% *mIoU*, surpassing all other methods [36, 14, 28, 31], including those with larger backbones. Notably, our method outperforms FB-Occ [17] by a significant margin of 2.17% *mIoU*. Most importantly, while our inference time of 77.9ms is slightly slower than FastOcc [12], we achieve a remarkable performance gain of 5.35% *mIoU* over their method. This result demonstrates that ProtoOcc achieves both high efficiency and superior accuracy, making it suitable for real-time applications.

Table 3 presents the performance analysis of multi-frame methods on the Occ3D-nuScenes validation set [24], utilizing the *mIoU* metric. ProtoOcc establishes a new state-of-the-art performance, exhibiting substantial improvements over existing methods [16, 12, 27, 13, 17], outperforming the previous best model, COTR [21], by 0.57% *mIoU*.

DBE	PQD	RPL	mIoU	Latency (ms)
			34.18	60.0
✓			35.87(+1.69)	75.7
	✓		35.63(+1.45)	61.1
✓	✓		37.05(+2.87)	77.9
✓	✓	✓	37.45(+3.27)	77.9

Table 4: Ablation study of main components of ProtoOcc.

4.3. Ablation Study

We performed an ablation study to evaluate the contributions of the components proposed in ProtoOcc. We trained on a quarter of the dataset for 24 epochs and evaluated the entire validation set using a ResNet-50 backbone [11] with a 256×704 resolution and a single frame.

Contributions of Main Components. Table 4 shows the impact of our main modules. The first row denotes a baseline employing 3D CNNs with small kernel sizes for both the encoder and the decoder. When adding DBE into the baseline, we achieved a notable 1.69% increase in *mIoU*. This demonstrates that DBE effectively combines local details from 3D CNNs with small-kernel sizes in the voxel branch with long-range spatial relationships from 2D CNNs with large-kernel sizes in the BEV branch. We integrated PQD into the baseline, achieving a 1.45% *mIoU* improvement while maintaining latency. This demonstrates that PQD effectively captures class properties through prototypes, enhancing performance without iterative query decoding. Incorporating both DBE and PQD surpasses the baseline by 2.87% in *mIoU*, demonstrating the effective combination of these components that leads to significant performance gains with minimal impact on latency. RPL further increases *mIoU* by 0.4% and enhances the model’s robustness by mitigating the impact of inaccurate class-specific masks.

Contributions of Dual Branch Encoder. We investigate the impact of the dual branch architecture with a large receptive field. As depicted in Table 5, model (e) utilizes DBE

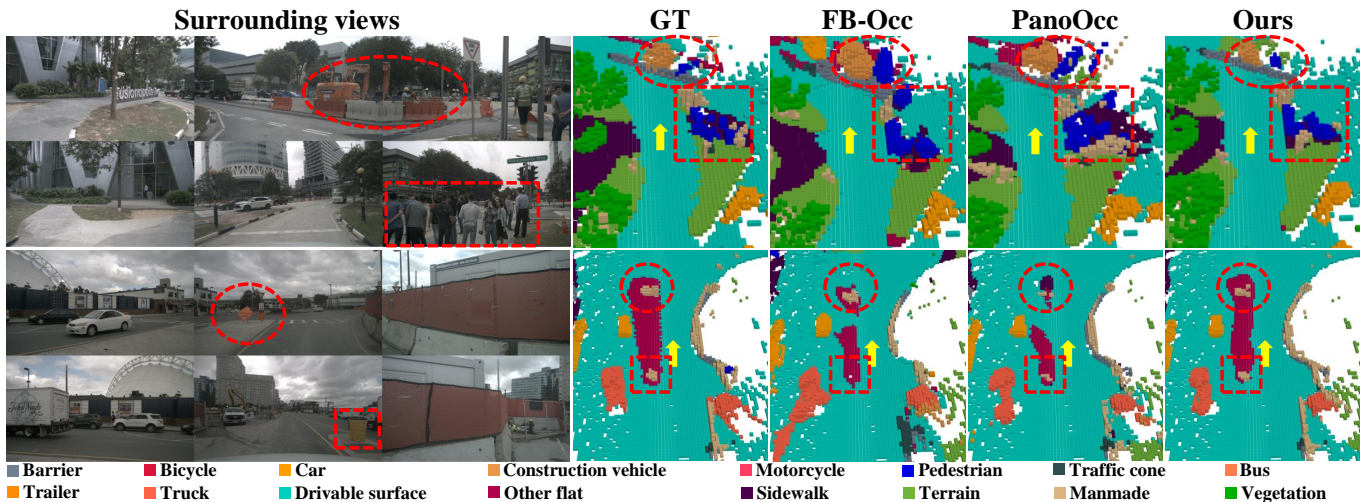


Figure 5: Qualitative results on the nuScenes validation set. The regions marked by red ellipses and rectangles emphasize the superior results generated by our proposed model. The yellow arrow indicates the position and direction of the ego vehicle.

Branch	Model	Voxel Kernel	BEV Kernel	MS Fusion	mIoU	Latency (ms)
Voxel Only	(a)	3			35.71	60.7
	(b)	7			36.14	87.2
BEV Only	(c)		3		35.64	52.0
	(d)		7		36.07	55.1
Dual Branch	(e)	3	3		36.70	71.1
	(f)	3	3	✓	36.93	74.5
	(Ours)	3	7	✓	37.45	77.9

Table 5: Ablation study of dual branch architecture. The "MS Fusion" means using multi-scale fusion in HFM.

with small kernel sizes and achieves a higher *mIoU* compared to models (a) and (c) that employ only a single representation. This result shows the effectiveness of leveraging dual representation. Multi-scale fusion in the model (f) further boosts *mIoU* by 0.23% over the model (e). When expanding the kernel size in each domain, model (b) increases the significant latency, whereas model (d) shows a smaller increase. Notably, by expanding the kernel size in the BEV domain, model (Ours) achieves a substantial 0.52% *mIoU* improvement over model (f) with only a minimal latency increase. This demonstrates the strength of DBE in effectively capturing both fine-grained 3D structures and long-range spatial relationships across various scales.

Impact of the Prototype Query Decoder. Table 6 presents an ablation study of decoder types, comparing *mIoU* and latency. While query-based decoders [36] achieve higher performance compared to CNN-based decoders, this comes with a trade-off of significantly increased latency. When adding AdaPG into the CNN-based decoder, we achieved competitive performance and faster latency than query-based decoders. Surprisingly, the combination of AdaPG and AgnoPG not only outperforms the query-based decoder by 0.79% in *mIoU* but also achieves latency that is

Decoder Type	AdaPG	AgnoPG	Iterative Decoding	mIoU	Latency (ms)
CNN-based				35.87	76.1
Query-based			✓	36.66	151.6
PQD	✓			36.87	77.4
	✓	✓		37.45	77.9

Table 6: Ablation study of decoder type.

73.7ms lower. This result demonstrates that PQD effectively captures the semantics of each class while efficiently calculating without iterative query decoding.

4.4. Qualitative Analysis

Figure 5 presents the qualitative results produced by the proposed ProtoOcc. We compare our method with existing approaches. Note that ProtoOcc yields notably better occupancy prediction results than others.

5. Conclusion

In this paper, we introduced an efficient encoder-decoder framework for the 3D occupancy prediction called ProtoOcc. DBE enhances the performance of the encoder by combining voxel and BEV representations and capturing fine-grained interactions while efficiently modeling long-range spatial relationships. Subsequently, PQD utilizes Scene-Adaptive and Scene-Agnostic Prototypes as queries to eliminate the need for iterative decoding process, significantly reducing computational complexity. We also proposed RPL to improve the model's robustness against inaccuracies in prototypes. Our method achieves state-of-the-art performance while significantly improving inference speed on the Occ3D-nuScenes benchmark.

References

- [1] Maxim Berman, Amal Rannen Triki, and Matthew B Blaschko. The lovász-softmax loss: A tractable surrogate for the optimization of the intersection-over-union measure in neural networks. In *Proceedings of the IEEE conference on computer vision and pattern recognition*, pages 4413–4421, 2018.
- [2] Zhaowei Cai, Avinash Ravichandran, Subhransu Maji, Charless Fowlkes, Zhuowen Tu, and Stefano Soatto. Exponential moving average normalization for self-supervised and semi-supervised learning. In *Proceedings of the IEEE/CVF Conference on Computer Vision and Pattern Recognition*, pages 194–203, 2021.
- [3] Anh-Quan Cao, Angela Dai, and Raoul de Charette. Pasco: Urban 3d panoptic scene completion with uncertainty awareness. In *Proceedings of the IEEE/CVF Conference on Computer Vision and Pattern Recognition*, pages 14554–14564, 2024.
- [4] Anh-Quan Cao and Raoul De Charette. Monoscene: Monocular 3d semantic scene completion. In *Proceedings of the IEEE/CVF Conference on Computer Vision and Pattern Recognition*, pages 3991–4001, 2022.
- [5] Qiang Chen, Xiaokang Chen, Jian Wang, Shan Zhang, Kun Yao, Haocheng Feng, Junyu Han, Errui Ding, Gang Zeng, and Jingdong Wang. Group detr: Fast detr training with group-wise one-to-many assignment. In *Proceedings of the IEEE/CVF International Conference on Computer Vision*, pages 6633–6642, 2023.
- [6] Yukang Chen, Jianhui Liu, Xiangyu Zhang, Xiaojuan Qi, and Jiaya Jia. Largekernel3d: Scaling up kernels in 3d sparse cnns. In *Proceedings of the IEEE/CVF Conference on Computer Vision and Pattern Recognition*, pages 13488–13498, 2023.
- [7] Bowen Cheng, Ishan Misra, Alexander G Schwing, Alexander Kirillov, and Rohit Girdhar. Masked-attention mask transformer for universal image segmentation. In *Proceedings of the IEEE/CVF conference on computer vision and pattern recognition*, pages 1290–1299, 2022.
- [8] Xiaohan Ding, Xiangyu Zhang, Jungong Han, and Guiguang Ding. Scaling up your kernels to 31x31: Revisiting large kernel design in cnns. In *Proceedings of the IEEE/CVF conference on computer vision and pattern recognition*, pages 11963–11975, 2022.
- [9] Alexey Dosovitskiy, Lucas Beyer, Alexander Kolesnikov, Dirk Weissenborn, Xiaohua Zhai, Thomas Unterthiner, Mostafa Dehghani, Matthias Minderer, Georg Heigold, Sylvain Gelly, et al. An image is worth 16x16 words: Transformers for image recognition at scale. *arXiv preprint arXiv:2010.11929*, 2020.
- [10] Yuxin Fang, Shusheng Yang, Shijie Wang, Yixiao Ge, Ying Shan, and Xinggang Wang. Unleashing vanilla vision transformer with masked image modeling for object detection. In *Proceedings of the IEEE/CVF International Conference on Computer Vision*, pages 6244–6253, 2023.
- [11] Kaiming He, Xiangyu Zhang, Shaoqing Ren, and Jian Sun. Deep residual learning for image recognition. In *Proceedings of the IEEE conference on computer vision and pattern recognition*, pages 770–778, 2016.
- [12] Jiawei Hou, Xiaoyan Li, Wenhao Guan, Gang Zhang, Di Feng, Yuheng Du, Xiangyang Xue, and Jian Pu. Fastocc: Accelerating 3d occupancy prediction by fusing the 2d bird’s-eye view and perspective view. *arXiv preprint arXiv:2403.02710*, 2024.
- [13] Junjie Huang, Guan Huang, Zheng Zhu, Yun Ye, and Dalong Du. Bevdet: High-performance multi-camera 3d object detection in bird-eye-view. *arXiv preprint arXiv:2112.11790*, 2021.
- [14] Yuanhui Huang, Wenzhao Zheng, Yunpeng Zhang, Jie Zhou, and Jiwen Lu. Tri-perspective view for vision-based 3d semantic occupancy prediction. In *Proceedings of the IEEE/CVF conference on computer vision and pattern recognition*, pages 9223–9232, 2023.
- [15] Yiming Li, Zhiding Yu, Christopher Choy, Chaowei Xiao, Jose M Alvarez, Sanja Fidler, Chen Feng, and Anima Anandkumar. Voxformer: Sparse voxel transformer for camera-based 3d semantic scene completion. In *Proceedings of the IEEE/CVF conference on computer vision and pattern recognition*, pages 9087–9098, 2023.
- [16] Zhiqi Li, Wenhao Wang, Hongyang Li, Enze Xie, Chonghao Sima, Tong Lu, Yu Qiao, and Jifeng Dai. Bevformer: Learning bird’s-eye-view representation from multi-camera images via spatiotemporal transformers. In *European conference on computer vision*, pages 1–18. Springer, 2022.
- [17] Zhiqi Li, Zhiding Yu, David Austin, Mingsheng Fang, Shiyi Lan, Jan Kautz, and Jose M Alvarez. Fb-occ: 3d occupancy prediction based on forward-backward view transformation. *arXiv preprint arXiv:2307.01492*, 2023.
- [18] Tsung-Yi Lin, Priya Goyal, Ross Girshick, Kaiming He, and Piotr Dollár. Focal loss for dense object detection. In *Proceedings of the IEEE international conference on computer vision*, pages 2980–2988, 2017.
- [19] Haisong Liu, Haiguang Wang, Yang Chen, Zetong Yang, Jia Zeng, Li Chen, and Limin Wang. Fully sparse 3d panoptic occupancy prediction. *arXiv preprint arXiv:2312.17118*, 2023.
- [20] Zhuang Liu, Hanzi Mao, Chao-Yuan Wu, Christoph Feichtenhofer, Trevor Darrell, and Saining Xie. A convnet for the 2020s. In *Proceedings of the IEEE/CVF conference on computer vision and pattern recognition*, pages 11976–11986, 2022.
- [21] Qihang Ma, Xin Tan, Yanyun Qu, Lizhuang Ma, Zhizhong Zhang, and Yuan Xie. Cotr: Compact occupancy transformer for vision-based 3d occupancy prediction. In *Proceedings of the IEEE/CVF Conference on Computer Vision and Pattern Recognition*, pages 19936–19945, 2024.
- [22] Jonah Philion and Sanja Fidler. Lift, splat, shoot: Encoding images from arbitrary camera rigs by implicitly

- unprojecting to 3d. In *Computer Vision–ECCV 2020: 16th European Conference, Glasgow, UK, August 23–28, 2020, Proceedings, Part XIV 16*, pages 194–210. Springer, 2020.
- [23] Pin Tang, Zhongdao Wang, Guoqing Wang, Jilai Zheng, Xiangxuan Ren, Bailan Feng, and Chao Ma. Sparseocc: Rethinking sparse latent representation for vision-based semantic occupancy prediction. In *Proceedings of the IEEE/CVF Conference on Computer Vision and Pattern Recognition*, pages 15035–15044, 2024.
- [24] Xiaoyu Tian, Tao Jiang, Longfei Yun, Yucheng Mao, Huitong Yang, Yue Wang, Yilun Wang, and Hang Zhao. Occ3d: A large-scale 3d occupancy prediction benchmark for autonomous driving. *Advances in Neural Information Processing Systems*, 36, 2024.
- [25] Wenwen Tong, Chonghao Sima, Tai Wang, Li Chen, Silei Wu, Hanming Deng, Yi Gu, Lewei Lu, Ping Luo, Dahua Lin, et al. Scene as occupancy. In *Proceedings of the IEEE/CVF International Conference on Computer Vision*, pages 8406–8415, 2023.
- [26] Xiaofeng Wang, Zheng Zhu, Wenbo Xu, Yunpeng Zhang, Yi Wei, Xu Chi, Yun Ye, Dalong Du, Jiwen Lu, and Xingang Wang. Openoccupancy: A large scale benchmark for surrounding semantic occupancy perception. In *Proceedings of the IEEE/CVF International Conference on Computer Vision*, pages 17850–17859, 2023.
- [27] Yuqi Wang, Yuntao Chen, Xingyu Liao, Lue Fan, and Zhaoxiang Zhang. Panoocc: Unified occupancy representation for camera-based 3d panoptic segmentation. In *Proceedings of the IEEE/CVF conference on computer vision and pattern recognition*, pages 17158–17168, 2024.
- [28] Yi Wei, Linqing Zhao, Wenzhao Zheng, Zheng Zhu, Jie Zhou, and Jiwen Lu. Surroundocc: Multi-camera 3d occupancy prediction for autonomous driving. In *Proceedings of the IEEE/CVF International Conference on Computer Vision*, pages 21729–21740, 2023.
- [29] Sanghyun Woo, Shoubhik Debnath, Ronghang Hu, Xinlei Chen, Zhuang Liu, In So Kweon, and Saining Xie. Convnext v2: Co-designing and scaling convnets with masked autoencoders. In *Proceedings of the IEEE/CVF Conference on Computer Vision and Pattern Recognition*, pages 16133–16142, 2023.
- [30] Zhuofan Xia, Xuran Pan, Shiji Song, Li Erran Li, and Gao Huang. Vision transformer with deformable attention. In *Proceedings of the IEEE/CVF conference on computer vision and pattern recognition*, pages 4794–4803, 2022.
- [31] Junkai Xu, Liang Peng, Haoran Cheng, Linxuan Xia, Qi Zhou, Dan Deng, Wei Qian, Wenxiao Wang, and Deng Cai. Vampire: Regulating intermediate 3d features for vision-centric autonomous driving. *Proceedings of the AAAI Conference on Artificial Intelligence*, 2024.
- [32] Zichen Yu, Changyong Shu, Jiajun Deng, Kangjie Lu, Zongdai Liu, Jiangyong Yu, Dawei Yang, Hui Li, and Yan Chen. Flashocc: Fast and memory-efficient occupancy prediction via channel-to-height plugin. *arXiv preprint arXiv:2311.12058*, 2023.
- [33] Bowen Zhang, Zhi Tian, Quan Tang, Xiangxiang Chu, Xiaolin Wei, Chunhua Shen, et al. Segvit: Semantic segmentation with plain vision transformers. *Advances in Neural Information Processing Systems*, 35:4971–4982, 2022.
- [34] Haiming Zhang, Xu Yan, Dongfeng Bai, Jiantao Gao, Pan Wang, Bingbing Liu, Shuguang Cui, and Zhen Li. Radocc: Learning cross-modality occupancy knowledge through rendering assisted distillation. In *Proceedings of the AAAI Conference on Artificial Intelligence*, volume 38, pages 7060–7068, 2024.
- [35] Hao Zhang, Feng Li, Huaizhe Xu, Shijia Huang, Shilong Liu, Lionel M Ni, and Lei Zhang. Mp-former: Mask-piloted transformer for image segmentation. In *Proceedings of the IEEE/CVF Conference on Computer Vision and Pattern Recognition*, pages 18074–18083, 2023.
- [36] Yunpeng Zhang, Zheng Zhu, and Dalong Du. Occformer: Dual-path transformer for vision-based 3d semantic occupancy prediction. In *Proceedings of the IEEE/CVF International Conference on Computer Vision*, pages 9433–9443, 2023.
- [37] Linqing Zhao, Xiuwei Xu, Ziwei Wang, Yunpeng Zhang, Borui Zhang, Wenzhao Zheng, Dalong Du, Jie Zhou, and Jiwen Lu. Lowrankocc: Tensor decomposition and low-rank recovery for vision-based 3d semantic occupancy prediction. In *Proceedings of the IEEE/CVF Conference on Computer Vision and Pattern Recognition*, pages 9806–9815, 2024.
- [38] Qiu Zhou, Jinming Cao, Hanchao Leng, Yifang Yin, Yu Kun, and Roger Zimmermann. Sogdet: Semantic-occupancy guided multi-view 3d object detection. In *Proceedings of the AAAI Conference on Artificial Intelligence*, volume 38, pages 7668–7676, 2024.